Effect of axial load on the propagation of elastic waves in helical beams

Ahmed Frikha [a], Fabien Treyssède [a], Patrice Cartraud [b]

[a] *Laboratoire Central des Ponts et Chaussées, 44341 Bouguenais Cedex, BP 4129, France*
[b] *GeM, UMR CNRS 6183, École Centrale de Nantes, 1 rue de la Noë, 44 321 Nantes Cédex 3, France*

Helical structures are designed to support heavy loads, which can significantly affect the dynamic behaviour. This paper proposes a physical analysis of the effect of axial load on the propagation of elastic waves in helical beams. The model is based on the equations of motion of loaded helical Timoshenko beams. An eigensystem is obtained through a Fourier transform along the axis. The equations are made dimensionless for beams of circular cross section and the number of parameters governing the problem is reduced to four (helix angle, helix index, Poisson coefficient, and axial strain). A parametric study is conducted. The effect of loading is quantified in high, medium and low frequency ranges. Noting that the effect is significant in low frequencies, dispersion curves of stretched and compressed helical beams are presented for different helix angles and radii. This effect is greater as the helix angle increases. Both the effects of stress and geometry deformation are shown to be non negligible on elastic wave propagation.

1. Introduction

Helical structures are used in many engineering applications. Typical examples are helical springs, widely used in automotive and aeronautic industry, and steel multi wire cables, largely encountered in civil engineering. These structures are usually subjected to large loads.

For the design of helical springs, several studies have been conducted to understand the dynamic behaviour and calculate the first vibration modes. First without considering the effect of applied loads, the computation of vibration modes of helical beams with circular cross section has been performed based on analytical but approximate solutions [1], the finite element methods [2] or the assumed mode method [3] for instance. Another approach is the transfer matrix method, employed in [4,5]. An efficient numerical method for predicting the natural frequencies of helical springs has been developed in [6]. The dynamic stiffness method has been used by Pearson and Wittrick [7] to find an exact solution for vibration of helical springs with the Euler Bernoulli model. Lee and Thompson [8] used the same method, but with the Timoshenko beam model.

However, the first vibration modes of helical springs correspond to low frequency motions, which are strongly affected by the presence of applied axial loads. The vibration analyses of springs have hence been extended to account for load effects on the natural frequencies thanks to the finite element method [9], the dynamic stiffness matrix [8] or the transfer matrix method, used in [10,11]. However, as noticed in [12,17], Pearson's equations [10] do not reduce to equations for simpler rods when load terms are included. All these studies show the importance of considering axial loads, compressive in the analyses, for the computation of natural frequencies.

As far as elastic wave propagation is concerned, the literature on helical waveguides is rather scarce. An analytical beam model [13] as well as more general numerical approaches [14,15] has been recently proposed. In [16], a semi analytical finite element method has also been proposed for the analysis of guided wave propagation inside multi wire helical waveguides,

typically encountered in civil engineering. However, these studies neglect the presence of applied loads, whose effect remains unexplored on guided waves.

The aim of this paper is to investigate the effect of axial loads on the propagation of guided modes in helical waveguides. For simplicity, multi wire waveguides are not considered and the model is based on the equations of motion of Timoshenko loaded helical beams. Such a model is not valid at high frequencies, when high order modes become propagating, but constitutes a first step and can serve as a reference solution before the development of fully three dimensional models, as done in [14 16] without loads. A space Fourier transform along the helical axis is performed, yielding a wave propagation eigensystem whose zero determinant corresponds to the dispersion relationship. The equations are made dimensionless for beams of circular cross sections. The problem is then governed by four parameters, which are the helix angle, the dimensionless radius (helix index), the dimensionless axial load (axial strain) and the Poisson coefficient.

The applied loads act on the dynamics through two effects: the deformation of the geometry and the stress generated inside the structure. Both effects are included in the present analysis. The deformed helix parameters are calculated using a non linear model.

A parametric study is conducted in order to highlight the effect of axial loads, compressive or tensile, on waves for various helix angles and radii. Three frequency ranges are distinguished. A branch identification of dispersion curves is given for a better physical understanding of the different modes existing in helical waveguides. The effects of stress and deformation are also compared.

2. Model

2.1. Equations of motion for dynamics

One considers a helical beam with a circular cross section of radius r. The helix centreline is defined by its pitch angle α_0 and radius R_0 in the unloaded state. In the loaded state, the spring is subjected to a static axial force P and the pitch angle and radius become α and R respectively (see Fig. 1). The curvature κ and torsion τ are given by $\kappa = \cos^2\alpha/R$ and $\tau = \sin\alpha\cos\alpha/R$. The Serret Frenet basis $(\mathbf{e}_n, \mathbf{e}_b, \mathbf{e}_t)$ associated with the helix is shown in Fig. 1, where $\mathbf{e}_n$, $\mathbf{e}_b$ and $\mathbf{e}_t$ respectively denote the normal, binormal and tangent unit vectors. In this coordinate system, the static force is written as $[0,\ P\cos\alpha,\ P\sin\alpha]$ and the static moment as $[0, -PR\sin\alpha,\ PR\cos\alpha]$. P is taken positive when tensile.

In the framework of Timoshenko beam theory, the general equations governing the small perturbations of a helical beam subjected to a static axial load P are given by the following set of 12 equations which relate the forces and moments to the displacements and rotations [11,12,17]:

$$\frac{du_n}{ds} = \tau u_b - \kappa u_t + \phi_b + \frac{Q_n}{GA_n}, \tag{1}$$

$$\frac{du_b}{ds} = -\tau u_n - \phi_n + \frac{Q_b}{GA_b}, \tag{2}$$

$$\frac{du_t}{ds} = \kappa u_n + \frac{Q_t}{EA_t}, \tag{3}$$

$$\frac{d\phi_n}{ds} = \tau\phi_b - \kappa\phi_t + \frac{M_n}{EI_n}, \tag{4}$$

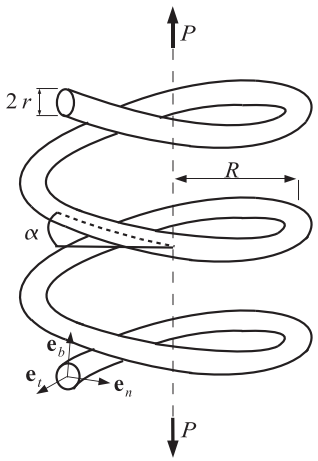

Fig. 1. Helical spring under axial load.

$$\frac{d\phi_b}{ds} = -\tau\phi_n + \frac{M_b}{EI_b}, \tag{5}$$

$$\frac{d\phi_t}{ds} = \kappa\phi_n + \frac{M_t}{GI_t}, \tag{6}$$

$$\begin{aligned}\frac{dQ_n}{ds} = &-\rho A_t\omega^2 u_n - P\sin\alpha\left(\frac{d\phi_b}{ds} + \frac{1}{GA_n}\frac{dQ_n}{ds} + \tau\phi_n - \tau\frac{Q_b}{GA_b}\right)\\ &+ P\cos\alpha\left(\frac{d\phi_t}{ds} - \kappa\phi_n + \kappa\frac{Q_b}{GA_b}\right) + \tau Q_b - \kappa Q_t,\end{aligned} \tag{7}$$

$$\frac{dQ_b}{ds} = -\rho A_t\omega^2 u_b + P\sin\alpha\left(\frac{d\phi_n}{ds} - \frac{1}{GA_b}\frac{dQ_b}{ds} - \tau\phi_b - \tau\frac{Q_n}{GA_n} + \kappa\phi_t\right) - \tau Q_n, \tag{8}$$

$$\frac{dQ_t}{ds} = -\rho A_t\omega^2 u_t - P\cos\alpha\left(\frac{d\phi_n}{ds} - \frac{1}{GA_b}\frac{dQ_b}{ds} - \tau\phi_b - \tau\frac{Q_n}{GA_n} + \kappa\phi_t\right) + \kappa Q_n, \tag{9}$$

$$\begin{aligned}\frac{dM_n}{ds} = &-\rho I_n\omega^2\phi_n + Q_b - PR\cos\alpha\left(\frac{d\phi_b}{ds} + \frac{1}{GA_n}\frac{dQ_n}{ds} + \tau\phi_n - \tau\frac{Q_b}{GA_b}\right)\\ &- PR\sin\alpha\left(\frac{d\phi_t}{ds} - \kappa\phi_n + \kappa\frac{Q_b}{GA_b}\right) + \tau M_b - \kappa M_t,\end{aligned} \tag{10}$$

$$\frac{dM_b}{ds} = -\rho I_b\omega^2\phi_b - Q_n + PR\cos\alpha\left(\frac{d\phi_n}{ds} - \frac{1}{GA_b}\frac{dQ_b}{ds} - \tau\phi_b - \tau\frac{Q_n}{GA_n} + \kappa\phi_t\right) - \tau M_n, \tag{11}$$

and

$$\frac{dM_t}{ds} = -\rho I_t\omega^2\phi_t + PR\sin\alpha\left(\frac{d\phi_n}{ds} - \frac{1}{GA_b}\frac{dQ_b}{ds} - \tau\phi_b - \tau\frac{Q_n}{GA_n} + \kappa\phi_t\right) + \kappa M_n. \tag{12}$$

where ω is the frequency, s is the curvilinear coordinate along the helix, $[u_n, u_b, u_t]$ denotes the dynamic displacement vector. $[\phi_n, \phi_b, \phi_t]$ is the rotation vector. $[Q_n, Q_b, Q_t]$ and $[M_n, M_b, M_t]$ are respectively the dynamic internal force and moment vectors. I_n, I_b and I_t define the second moments of area of the section about the Serret Frenet directions. For a circular cross section, $I_n = I_b = I_t/2 = \pi r^4/4$. A_n, A_b and A_t represent cross sections defined by: $A_n = A_b = \gamma A_t = \gamma\pi r^2$, where $\gamma = 6(1+\nu)/(7+6\nu)$ is the Timoshenko shear coefficient. The material characteristics are the material density ρ, the Young's modulus E, the shear modulus $G = E/2(1+\nu)$ and the Poisson coefficient ν.

Without axial load ($P = 0$), the above equations become identical to the equations presented by Wittrick [1]. As stated by this author, it is assumed that the condition $\kappa^2 I_t/A_t << 1$ is satisfied, or equivalently $(\kappa r)^2 << 1$, which means that the beam radius r must be rather small compared to the helix radius of curvature $1/\kappa$. Such a condition is usually fulfilled for springs. Also, it generally applies to helical wires constituting civil engineering cables because of their large pitch angle (often close to $\pi/2$).

2.2. Wave propagation eigensystem

In order to reduce the number of parameters, the variables of Eqs. (1) (12) are made dimensionless. r is chosen as the characteristic length and r/c_s as the characteristic time where c_s is the shear bulk velocity defined by $c_s^2 = G/\rho$. Stars will be used to denote dimensionless variables. The dimensional and dimensionless variables are related by:

$$s^* = \frac{s}{r}, u_j^* = \frac{u_j}{r}, \phi_j^* = \phi_j, Q_j^* = \frac{Q_j}{\pi\rho r^2 c_s^2}, M_j^* = \frac{M_j}{\pi\rho r^3 c_s^2}, j = n, b, t. \tag{13}$$

First, Eqs. (7) (12) are used to replace the forces and moments in Eqs. (1) (6). This enables to obtain a system of six linear equations, written in terms of the displacements and rotations. Then, the equations are made dimensionless thanks to Eq. (13). A Fourier transform along the s axis allows to replace $\partial/\partial s^*$ with iK, where $K = kr$ denotes the dimensionless wavenumber along the s axis. Finally, one gets the following 6×6 matrix system:

$$\left(\mathbf{A}_1 - \Omega^2\mathbf{A}_2 - iK\mathbf{B} + K^2\mathbf{C}\right)\mathbf{U} = 0. \tag{14}$$

where $\Omega = \omega r / c_s$ is the dimensionless frequency and the eigenvectors $\mathbf{U} = \{ u_n^* \quad u_b^* \quad u_t^* \quad \phi_n^* \quad \phi_b^* \quad \phi_t^* \}^T$ contains displacement and rotation components in the Serret Frenet basis. The matrices $\mathbf{A}_1$, $\mathbf{A}_2$, $\mathbf{B}$ and $\mathbf{C}$ are given by:

$$\mathbf{A}_2 = \mathrm{diag}(1, 1, 1, 1/4, 1/4, 1/2), \tag{15}$$

$$\mathbf{C} = \begin{bmatrix} \gamma + \sigma s & 0 & 0 & 0 & 0 & 0 \\ 0 & \gamma + \sigma s & 0 & 0 & 0 & 0 \\ 0 & -\sigma c & 2(1+\nu) & 0 & 0 & 0 \\ \sigma\delta c & 0 & 0 & (1+\nu)/2 & 0 & 0 \\ 0 & \sigma\delta c & 0 & 0 & (1+\nu)/2 & 0 \\ 0 & \sigma\delta s & 0 & 0 & 0 & 1/2 \end{bmatrix}, \tag{16}$$

$$\mathbf{A}_1 = [\, \mathbf{A}_{11} \quad \mathbf{A}_{12} \,], \tag{17}$$

$$\mathbf{B} = [\, \mathbf{B}_1 \quad \mathbf{B}_2 \,], \tag{18}$$

with the following submatrices:

$$\mathbf{A}_{11} = \begin{bmatrix} c^2\left(\gamma s^2 + 2(1+\nu)c^2 + \sigma s\right)/\delta^2 & 0 & 0 \\ 0 & s^2c^2(\gamma + \sigma s)/\delta^2 & -sc^3(\gamma + \sigma s)/\delta^2 \\ 0 & -sc^3(\gamma + \sigma s)/\delta^2 & c^4(\gamma + \sigma s)/\delta^2 \\ \gamma s c/\delta & 0 & 0 \\ 0 & sc\left(\gamma + \sigma s c^2\right)/\delta & -c^2\left(\gamma + \sigma s c^2\right)/\delta \\ 0 & \sigma s^3 c^2/\delta & -\sigma s^2 c^3/\delta \end{bmatrix}, \tag{19}$$

$$\mathbf{A}_{12} = \begin{bmatrix} \gamma s c/\delta & 0 & 0 \\ 0 & \gamma s c/\delta & \sigma s c^2/\delta \\ 0 & -\gamma c^2/\delta & -\sigma c^3/\delta \\ \gamma + c^2\left(1 + \nu s^2\right)/2\delta^2 & 0 & 0 \\ 0 & \gamma + (1+\nu)s^2c^2/2\delta^2 & -(1+\nu)sc^3/2\delta^2 + \sigma c^3 \\ 0 & -(1+\nu)sc^3/2\delta^2 & c^2\left((1+\nu)c^2/2\delta^2 + \sigma s\right) \end{bmatrix}, \tag{20}$$

$$\mathbf{B}_1 = \begin{bmatrix} 0 & -c\left(2\gamma s + \sigma\left(1 + s^2\right)\right)/\delta & c^2(\gamma + 2(1+\nu) + \sigma s)/\delta \\ 2sc(\gamma + \sigma s)/\delta & 0 & 0 \\ -c^2(\gamma + 2(1+\nu) + 2\sigma s)/\delta & 0 & 0 \\ 0 & -\left(\gamma + \sigma s c^2\right) & \sigma c^3 \\ \gamma + 2\sigma s c^2 & 0 & 0 \\ 2\sigma s^2 c & 0 & 0 \end{bmatrix}, \tag{21}$$

$$\mathbf{B}_2 = \begin{bmatrix} 0 & -\gamma & -\sigma c \\ \gamma & 0 & 0 \\ 0 & 0 & 0 \\ 0 & -(1+\nu)sc/\delta & (2+\nu)c^2/2\delta + \sigma\delta s \\ (1+\nu)sc/\delta & 0 & 0 \\ -(2+\nu)c^2/2\delta & 0 & 0 \end{bmatrix}, \tag{22}$$

where the parameters s, c, δ and σ are given by:

$$s = \sin\alpha, c = \cos\alpha, \delta = \frac{R}{r}, \sigma = \frac{P}{\pi\rho r^2 c_s^2}. \tag{23}$$

The solution of Eq. (14) yields the propagation modes. Eqs. (14) (22) show that wave propagation in axially loaded helical beams is governed by α (the helix angle), δ (dimensionless helix radius or helix index), σ (dimensionless axial load) and ν (Poisson coefficient). Hence, dispersion curves (K, Ω) only depend on these 4 dimensionless parameters.

For a given Ω, the eigenproblem (14) is quadratic in K. This problem can be recast into a generalised linear eigensystem written for $[U^T K U^T]^T$ in order to be solved by standard numerical solvers (see Tisseur et al. [18] for instance). One gets 12 wavenumbers. Purely real and imaginary wavenumbers corresponding respectively to propagating and evanescent modes, appear in pairs of opposite signs. Fully complex wavenumbers corresponding to inhomogeneous modes, appear in quadruples of complex conjugates and opposite signs. If interest is restricted to propagating modes only, one can set K (as a real wavenumber) and determine Ω. The eigenproblem (14) is then linear for finding Ω^2 and 6 positive eigenfrequencies are found for each real

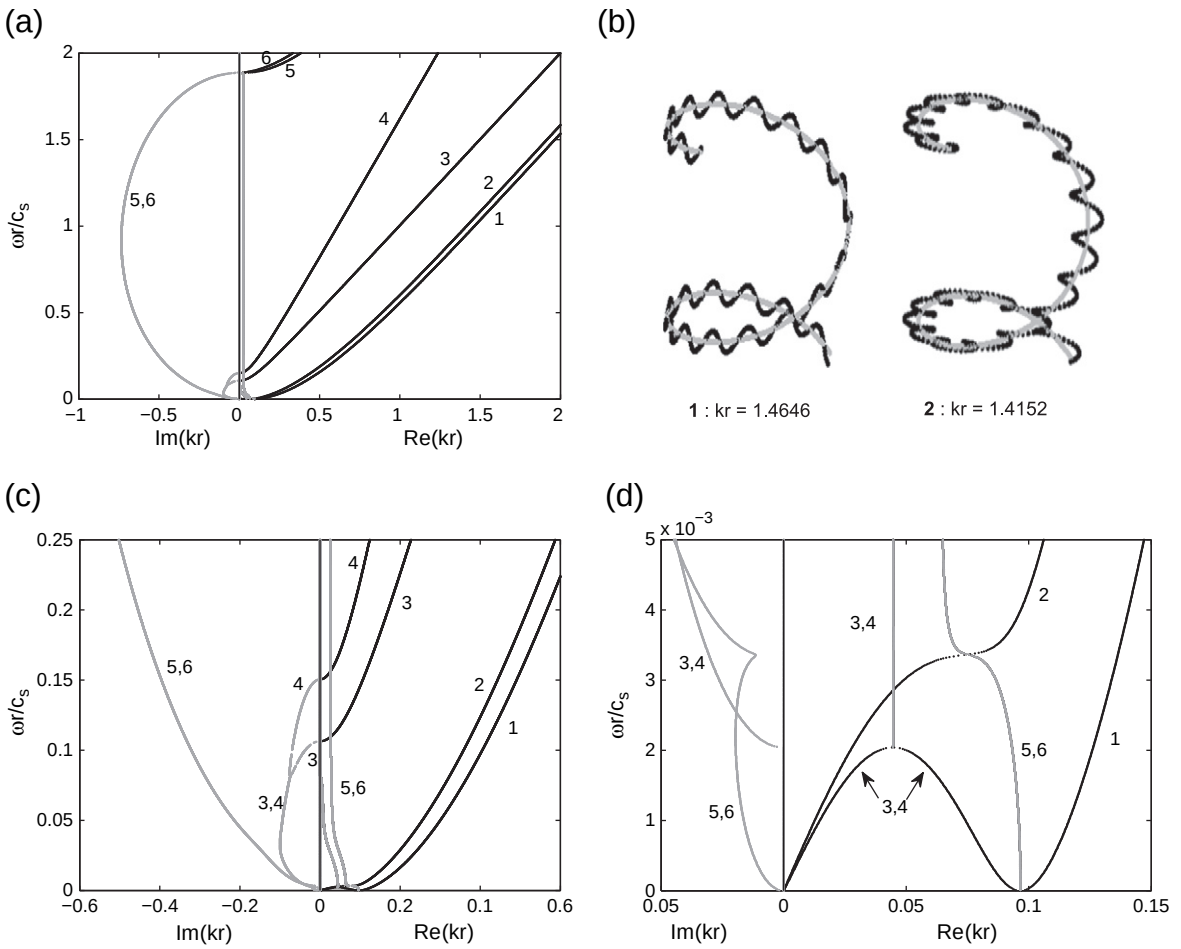

Fig. 2. Unloaded helical waveguide with $\delta_0 = 10$ and $\alpha_0 = 15^\circ$. (a), (c), (d): dispersion curves (grey lines: non-propagating modes, black lines: propagating modes). (b): modeshapes of modes 1 and 2 at $\omega r/cs = 1$ (grey lines: undeformed, black lines: deformed helix centreline).

wavenumber K. As a side remark, note that the eigenvalue problem (14) degenerates to that presented in the Appendix of Ref. [14] in the unloaded case ($\sigma = 0$).

2.3. Deformed helical geometry

The eigenvalue problem (14) is written in terms of α and δ, which are the helix pitch angle and index in the loaded state. Both are unknown and should be calculated provided the load, the initial angle α_0 and index δ_0 in the unloaded state. One considers a helical waveguide subjected to a given axial strain, denoted ϵ. One has $\epsilon = (l \sin\alpha - l_0 \sin\alpha_0)/l_0 \sin\alpha_0$, where l_0 and l are the curvilinear length of one helix step along the s axis in the unloaded state and loaded state respectively. We follow the same approach as the one proposed in Chapter 20 of [19], which proposes a non linear solution for large deflection under simplifying assumptions limited to sufficiently large index δ_0 (typically, $\delta_0 \geq 5$) and small pitch angle (which will be supposed for the results of this paper).[1] Shearing strains are neglected. The stretching of the helix centreline is neglected so that $l \simeq l_0$ [19,20]. Therefore, $\epsilon \simeq \sin\alpha/\sin\alpha_0 - 1$ and the angle α is simply obtained from:

$$\alpha = \arcsin((1+\epsilon)\sin\alpha_0). \tag{24}$$

Then following [19], the bending and torsional moments are respectively balanced by the change in curvature and torsion times the corresponding rigidities:

$$PR\sin\alpha = -EI_b\Delta\kappa, \tag{25}$$

[1] Note that such a solution is well suited for springs but would not be applicable for helical wires constituting civil engineering cables (usually of small index and large angle).

$$P\,R\cos\alpha = GI_t\Delta\tau \tag{26}$$

where $\Delta\kappa = \cos^2\alpha/R - \cos^2\alpha_0/R_0$ and $\Delta\tau = \sin\alpha\cos\alpha/R - \sin\alpha_0\cos\alpha_0/R_0$.

Eliminating P from these two equations, one obtains the following dimensionless expressions for δ, written in terms of α:

$$\delta = \frac{(1+\nu)\cos^2\alpha + \sin^2\alpha}{(1+\nu)\cos^2\alpha_0 + \sin\alpha_0\cos\alpha_0\tan\alpha}\delta_0. \tag{27}$$

From Eq. (25), the dimensionless load σ is finally given by:

$$\sigma = \frac{(1+\nu)}{2\delta\sin\alpha}\left(\frac{\cos^2\alpha_0}{\delta_0} - \frac{\cos^2\alpha}{\delta}\right). \tag{28}$$

In this paper, note that the parametric study given in the next section is conducted in terms of ϵ instead of σ.

As a side remark, the geometric parameters of the unloaded and loaded helical beam must satisfy the geometric conditions $\pi\,\delta_0\sin\alpha_0 > 1$ and $\pi\,\delta\sin\alpha > 1$, respectively (meaning that adjacent turns do not overlap each other).

3. Results

In this section, the unloaded case is first considered in order to clearly identify branch modes inside a typical spring. Three frequency ranges can be distinguished. Focusing on propagating modes, the effect of load on the wave propagation is studied in each frequency range. The effect of the dimensionless radius δ_0 and angle α_0 on the wave propagation in a loaded helical spring is finally examined. Numerical results are obtained with a Poisson coefficient ν of 0.3.

3.1. Branch identification

In this section, results are given for a helical beam with dimensionless radius δ_0 of 10 and angle α_0 of 15°. Fig. 2(a),(c),(d) shows the dispersion curves ($\omega r/c_s$ versus kr) of the unloaded helical beam for three frequency ranges: [0;2], [0;0.25] and [0;0.005].

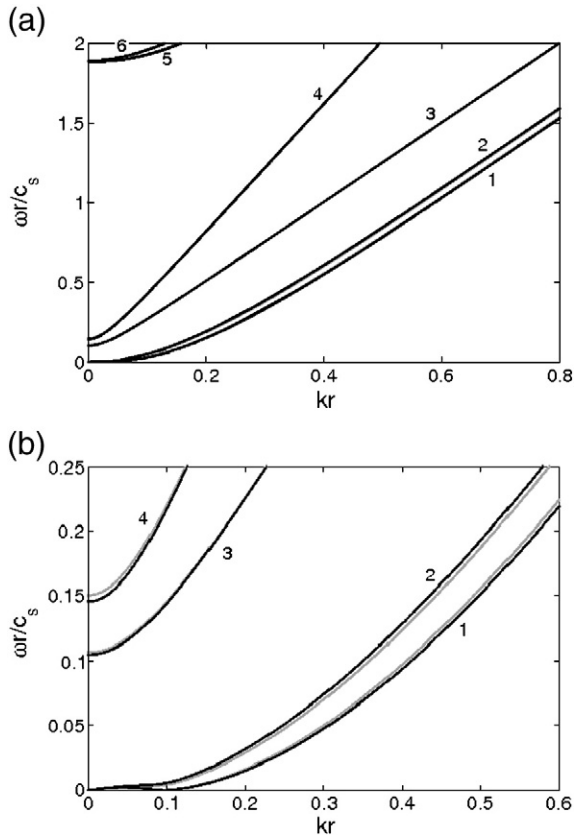

Fig. 3. Dispersion curves of the unloaded (grey lines) and loaded $\epsilon = 0.4$ (black lines) helical beams for $\delta_0 = 10$, $\alpha_0 = 15°$.

These three ranges correspond to three frequency regimes, typical for helical beams, as already identified in [13]. The eigensystem (14) is solved by fixing the dimensionless frequency in order to obtain propagating as well as non propagating modes, making easier the branch identification. At each frequency, there are six wavenumbers having a positive real part.

In order to determine their physical behaviour, a representation of modeshapes 1 and 2 is sketched in Fig. 2(b) for $\omega r/cs = 1$. It comes that both modes 1 and 2 have a flexural wave behaviour. Mode 1 mainly oscillates in the binormal direction while the motion of mode 2 is mainly in the normal direction. The modes 3 and 4 have not been sketched in the figure because their behaviour could be hardly identified with such a representation, which can only show displacement components normal to the beam neutral axis. Instead, the behaviour of these modes has been identified by inspecting the dominant component of eigenvectors. The dominant component of modes 3 and 4 was found to be ϕ_t^* and u_t^* respectively, indicating that mode 3 has a torsional behaviour while mode 4 is of compressional type. Similarly to the cylinder dispersion curves, modes 5 and 6 have a flexural wave behaviour of higher order (of no interest in this paper).

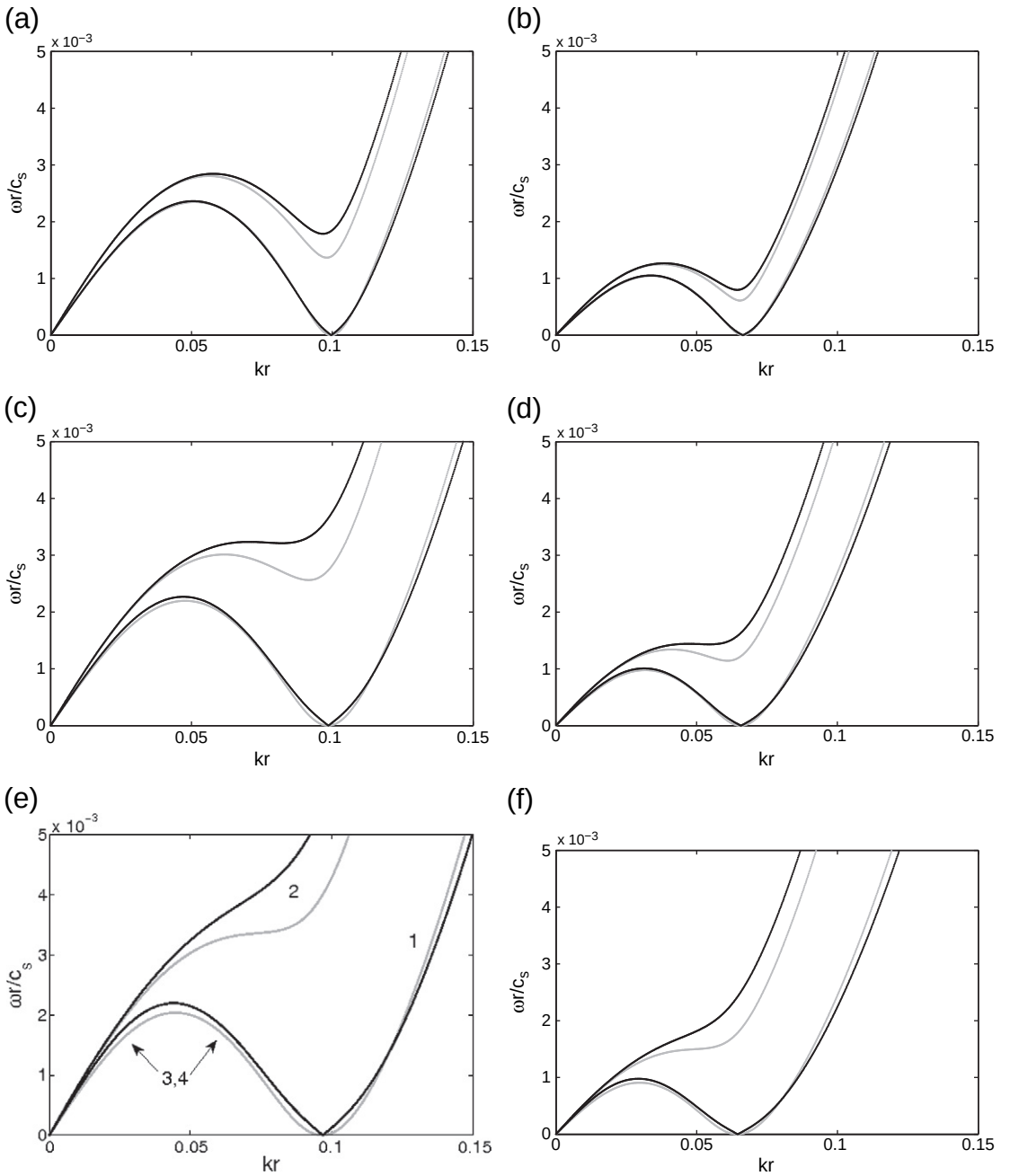

Fig. 4. Dispersion curves of unloaded (grey lines) and loaded $\epsilon = 0.4$ (black lines) helical beams in the low-frequency range for: (a) $\delta_0 = 10, \alpha_0 = 5^\circ$, (b) $\delta_0 = 15, \alpha = 5^\circ$, (c) $\delta_0 = 10, \alpha_0 = 10^\circ$, (d) $\delta_0 = 15, \alpha_0 = 10^\circ$, (e) $\delta_0 = 10, \alpha_0 = 15^\circ$, and (f) $\delta_0 = 15, \alpha_0 = 15^\circ$.

For a dimensionless frequency exceeding 1.88, all the six modes are propagating (see Fig. 2a). Under 1.88, modes 5 and 6 become inhomogeneous (complex wavenumbers). As shown in Fig. 2(c) and (d), the compressional mode (mode 4) is cut off for frequencies between 0.002 and 0.15 (Im(kr)>0), while the torsional mode (mode 3) is cut off between 0.002 and 0.106. Note that between 0.002 and 0.08, the wavenumbers of modes 3 and 4 are grouped together. Then below 0.002, modes 3 and 4 divide into two propagating modes, for which it becomes difficult to distinguish compressional from torsional behaviour. This difficulty was also mentioned in [13,14]. It can be noticed that one of these two modes has a curve of negative slope, indicating a backward propagation (positive wavenumber with negative group velocity $V_g = \partial\omega/\partial k$).

Now, a tensile deformation $\epsilon = 0.4$ is applied. One focuses on propagating modes only (we set kr and look for $\omega r/cs$). Fig. 3 shows the dispersion curves of propagating modes in the unloaded and loaded cases for the first two frequency ranges. The effect of loading is negligible for high frequencies (above 0.25). For medium frequencies (below 0.25), there is small differences (few percents) between the unloaded and loaded curves. These differences are localised near the cut off frequencies of the torsional

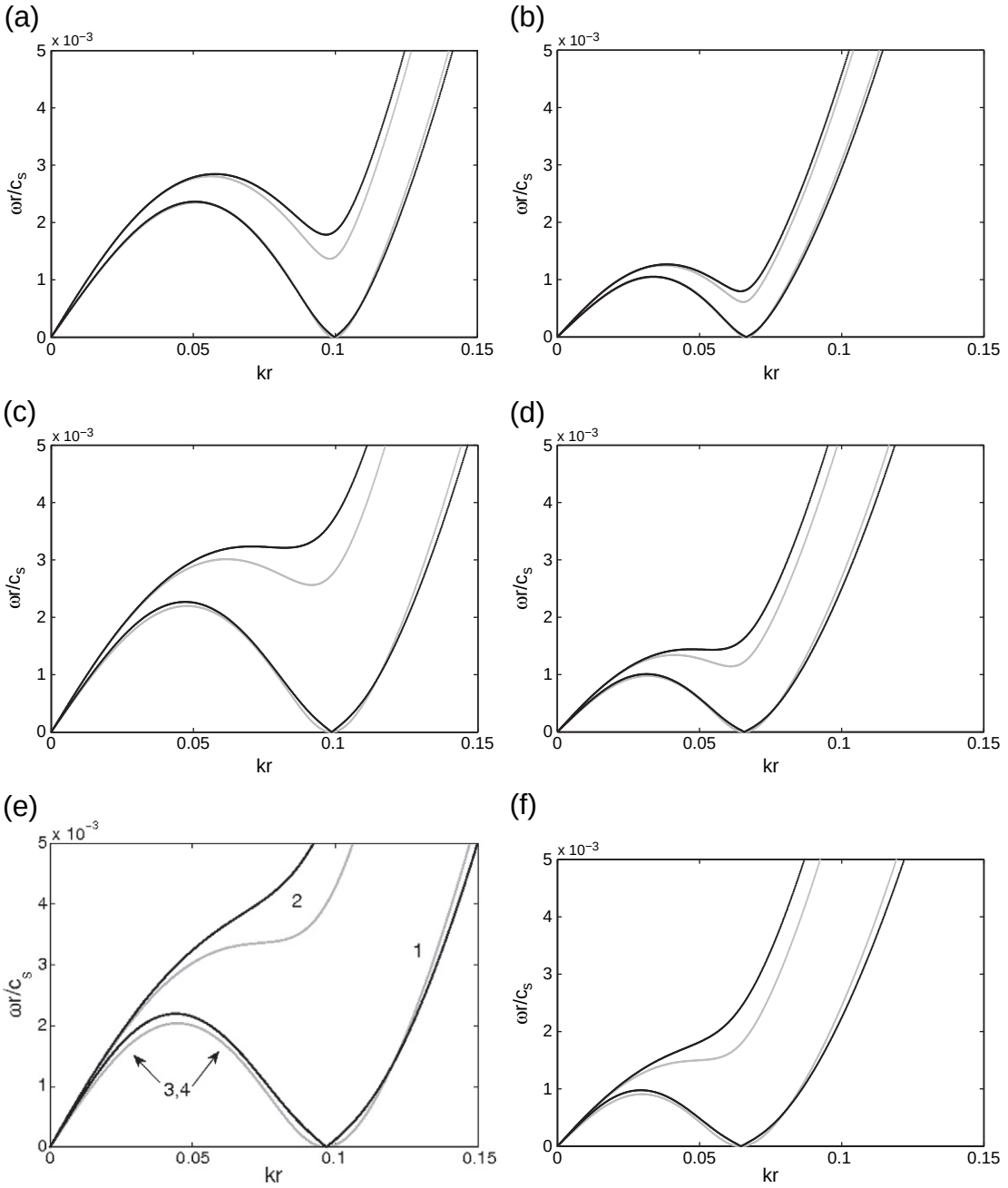

Fig. 5. Dispersion curves of unloaded (grey lines) and loaded $\epsilon =$ 0.4 (black lines) helical beams in the low-frequency range for: (a) $\delta_0 = 10, \alpha_0 = 5^\circ$, (b) $\delta_0 = 15, \alpha = 5^\circ$, (c) $\delta_0 = 10, \alpha_0 = 10^\circ$, (d) $\delta_0 = 15, \alpha_0 = 10^\circ$, (e) $\delta_0 = 10, \alpha_0 = 15^\circ$, and (f) $\delta_0 = 15, \alpha_0 = 15^\circ$.

and compressional modes (modes 3 and 4 respectively), both increasing under tensile loads. Note that these cut off frequencies shift higher as the helix angle increases and would decrease under compressive loads (results not shown for conciseness). Despite the significant value of the axial deformation on the helical beam, the effect of loading becomes significant only in the low frequency range, as shown in the next subsection.

3.2. Effect of loading in the low frequency range

A parametric study is conducted in order to analyse the effect of loading for low frequencies (below 0.005). Fig. 4 shows the superposition of dispersion curves of unstretched ($\epsilon = 0$) and stretched helical beams ($\epsilon = 0.4$). The effect of loading has been studied for six different helical beams, having dimensionless radii δ_0 of 10, 15 and angles α_0 of 5°, 10°, 15°. The tensile load has an effect on the four propagating modes. For clarity, Fig. 4(e) shows the mode labels as previously identified. The load effect is found to be the most important for mode 2 (flexural mode oscillating in the normal direction), its dispersion curve shifting to higher frequencies. The other flexural mode (mode 1) is less sensitive to the load, with a shift to lower frequencies (except near the rigid body point, corresponding to a zero frequency). As far as the longitudinal and torsional modes are concerned (modes 3 and 4), their frequency slightly increase under tensile load. As can be observed in Fig. 4, the applied load has a greater effect as the helix angle increases.

Fig. 5 shows the same results as Fig. 4 for the compressive case $\epsilon = -0.4$. One observes the same trend as before but in the opposite direction. For instance, modes 2, 3 and 4 shift to lower frequencies. When the load is compressive, there exists an interval of wavenumbers corresponding to long waves for which $Re(\omega) = 0$. In this interval, the corresponding frequencies are not strictly zero but have a small imaginary part. This indicates that compressed helical beams are incapable of transmitting these waves. Note that the same phenomenon was found in compressed arches [21]. For helical beams, this interval is greater as the helix angle or the load increase and as the index decreases.

In practice, it can be of interest to evaluate how significant are the stress levels inside the beam. Quantitatively, the maximum shearing stress at the surface of the beam can be approximated as $2PR/\pi r^3$ (see Chapters 19 and 20 of Ref. [19]). From Eq. (23), this stress is equal to $2\delta\sigma E/2(1+nu)$, where δ and σ are obtained from Eqs. (27) and (28). Let us choose $E = 2.0e11$ Pa (typical value for steel). Then in Figs. 4 and 5, applying $|\epsilon| = 0.4$ would yield a maximum shearing stress varying between 180 MPa

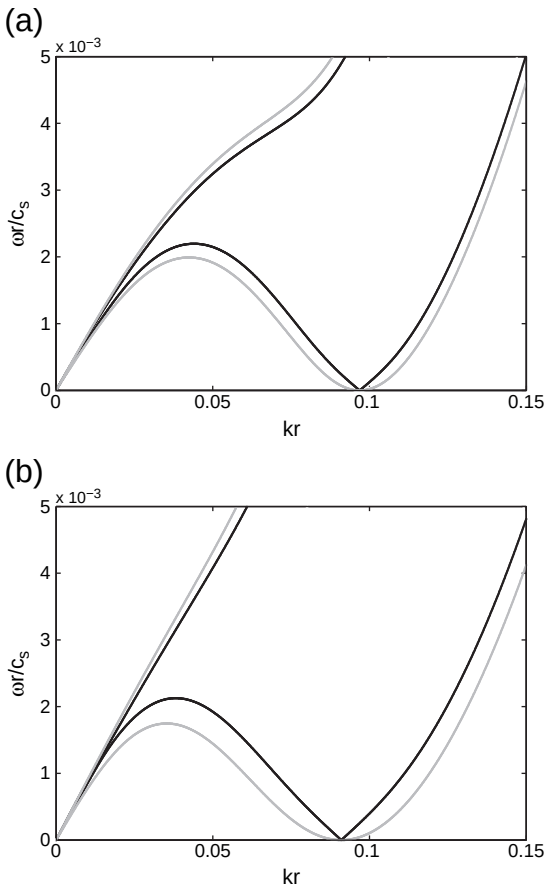

Fig. 6. Dispersion curves of the deformed helical beam including the effect of stress (black) and without (grey) for $\epsilon = 0.4$, $\delta_0 = 10$ and: (a) $\alpha_0 = 15°$, (b) $\alpha_0 = 25°$.

(corresponding to the case $\delta_0 = 15$, $\alpha_0 = 5^\circ$) and 830 MPa (for $\delta_0 = 10$, $\alpha_0 = 15^\circ$). Note that the stress inside the beam must not exceed the elastic limit (which depends on the material considered), otherwise the theory used in this paper would be no longer applicable.

3.3. Note on the effect of stress versus deformation

The theory presented in Section 2 shows that the axial load acts upon the dynamic equilibrium equations through two combined effects: the deformation of the geometry (from (δ_0, α_0) to (δ, α)) and the generation of stress ($\sigma \neq 0$). In Section 3.2, both effects were taken into account. In the present section, we are interested in evaluating the influence of stress compared to the deformation. As an example, Fig. 6 compares the loaded dispersion curves of Fig. 4 (e) with the curves obtained by neglecting stress, i.e. arbitrarily setting σ to zero (the deformation of the geometry is still taken into account).

The stress σ has an effect that cannot be neglected. Comparing Fig. 6 (a) with Fig. 4 (e), this effect is opposed to, but lower than, the effect caused by the geometry deformation. With the same applied deformation and dimensionless radius, the effect of stress is more important with the increase of the helix angle. This phenomenon can be observed by comparing Fig. 6 (a) to (b).

It can be concluded that both effects of stress and geometry deformation should be considered to study the effect of load on the propagation of elastic waves in helical beams.

4. Conclusions

Elastic wave propagation in a helical beam subjected to a compressive or tensile axial load has been analysed. The deformation of the geometry under the applied axial load has been taken into account in the calculation of wave propagation. The effect of load on wave propagation has been highlighted for high, medium and low frequency ranges. A branch identification of dispersion curves has been performed for both propagating and non propagating modes. The effect of loading is significant on the four propagating modes in a low frequency range. The dispersion curve of the flexural mode oscillating in the normal direction shifts to higher frequencies under tensile loads and vice versa for compressive loads. The loading effect is less important for the three other propagating modes. The applied load has a greater effect as the helix increases. Both the effects of stress and geometry deformation are found to be non negligible and should be considered in the analysis of elastic wave propagation in axially loaded helical beams.

References

[1] W.H. Wittrick, On elastic wave propagation in helical springs, Int. J. Mech. Sci. 8 (1966) 25–47.
[2] J.E. Mottershead, Finite elements for dynamical analysis of helical rods, Int. J. Mech. Sci. 22 (1980) 267–283.
[3] A. Ward, M.S. Towers, H.A. Barker, Dynamic analysis of helical springs by the assumed mode method, J. Sound Vib. 112 (2) (1987) 305–320.
[4] V. Yildirim, Investigation of parameters affecting free vibration frequency of helical springs, Int. J. Numer. Methods Eng. 39 (1) (1996) 99–114.
[5] V. Yildirim, N. Ince, Natural frequencies of helical springs of arbitrary shape, J. Sound Vib. 204 (2) (1997) 311–329.
[6] V. Yildirim, An efficient numerical method for predicting the natural frequencies of cylindrical helical springs, Int. J. Mech. Sci. 41 (1999) 919–939.
[7] D. Pearson, W.H. Wittrick, An exact solution for the vibration of helical springs using a Bernoulli–Euler model, Int. J. Mech. Sci. 28 (2) (1986) 83–96.
[8] J. Lee, D.J. Thompson, Dynamic stiffness formulation, free vibration and wave motion of helical springs, J. Sound Vib. 239 (2001) 297–320.
[9] Y. Xiong, B. Tabarrok, A finite element model for the vibration of spatial rods under various applied loads, Int. J. Mech. Sci. 34 (1992) 41–51.
[10] D. Pearson, Transfer matrix method for the vibration of compressed helical springs, J. Mech. Eng. 24 (1982) 163–171.
[11] L.-E. Becker, G.-G. Chassie, W.L. Cleghorn, On the natural frequencies of helical compression springs, Int. J. Mech. Sci. 44 (2002) 825–841.
[12] L.E. Becker, W.L. Cleghorn, On the buckling of helical compression springs, Int. J. Mech. Sci. 34 (1992) 275–282.
[13] S.V. Sorokin, Linear dynamic of elastic helical sprigs: asymptotic analysis of wave propagation, Proc. R. Soc. A 465 (2009) 1513–1537.
[14] F. Treyssède, Numerical investigation of elastic modes of propagation in helical waveguides, J. Acoust. Soc. Am. 121 (2007) 3398–3408.
[15] F. Treyssède, Elastic waves in helical waveguides, Wave Motion 45 (2008) 457–470.
[16] F. Treyssède, L. Laguerre, Investigation of elastic modes propagating in multi-wire helical waveguides, J. Sound Vib. 329 (2010) 1702–1716.
[17] G.G. Chassie, L.E. Becker, W.L. Cleghorn, On the buckling of helical springs under combined compression and torsion, Int. J. Mech. Sci. 39 (1997) 697–704.
[18] F. Tisseur, K. Meerbergen, The quadratic eigenvalue problem, SIAM Rev. 43 (2001) 235–286.
[19] A.M. Wahl, Mechanical Springs, Second edition, Mc Graw-Hill, Inc, New York, 1963.
[20] J.A. Haringx, On highly compressible helical springs and rubber rods, and their application for vibration-free mountings, Philips Res. Rep. 3 (1948) 401–449.
[21] M. Farshad, Wave propagation in prestressed curved rods, J. Eng. Mech. Div. 106 (1980) 395–408.